NANO LETTERS

Letter

pubs.acs.org/NanoLett

Effects of Polytypism on Optical Properties and Band Structure of Individual Ga(N)P Nanowires from Correlative Spatially Resolved Structural and Optical Studies

Alexander Dobrovolsky,[†] Per O. Å. Persson,[†] Supanee Sukrittanon,[‡] Yanjin Kuang,[§] Charles W. Tu,[∥] Weimin M. Chen,[†] and Irina A. Buyanova*[,†]

[†]Department of Physics, Chemistry and Biology, Linköping University, S-581 83 Linköping, Sweden

[‡]Graduate Program of Materials Science and Engineering, [§]Department of Physics, and [∥]Department of Electrical and Computer Engineering, University of California, La Jolla, California 92093, United States

Supporting Information

ABSTRACT: III−V semiconductor nanowires (NWs) have gained significant interest as building blocks in novel nanoscale devices. The one-dimensional (1D) nanostructure architecture allows one to extend band structure engineering beyond quantum confinement effects by utilizing formation of different crystal phases that are thermodynamically unfavorable in bulk materials. It is therefore of crucial importance to understand the influence of variations in the NWs crystal structure on their fundamental physical properties. In this work we investigate effects of structural polytypism on the optical properties of gallium phosphide and GaP/GaNP core/shell NW structures by a correlative investigation on the structural and optical properties of individual NWs. The former is monitored by transmission electron microscopy, whereas the latter is studied via cathodoluminescence (CL) mapping. It is found that structural defects, such as rotational twins in zinc blende (ZB) GaNP, have detrimental effects on light emission intensity at low temperatures by promoting nonradiative recombination processes. On the other hand, formation of the wurtzite (WZ) phase does not notably affect the CL intensity neither in GaP nor in the GaNP alloy. This suggests that zone folding in WZ GaP does not enhance its radiative efficiency, consistent with theoretical predictions. We also show that the change in the lattice structure have negligible effects on the bandgap energies of the GaNP alloys, at least within the range of the investigated nitrogen compositions of <2%. Both WZ and ZB GaNP are found to have a significantly higher efficiency of radiative recombination as compared with that in parental GaP, promising for potential applications of GaNP NWs as efficient nanoscale light emitters within the desirable amber-red spectral range.

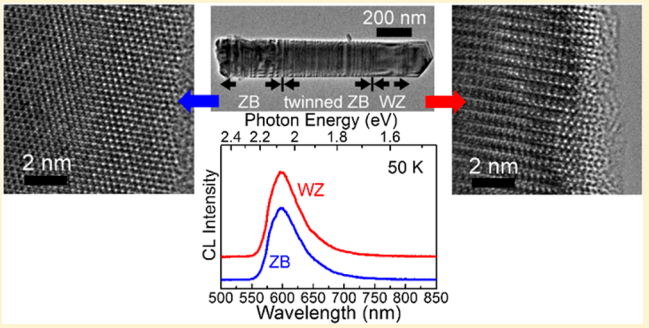

KEYWORDS: *Gallium phosphide, GaNP, nanowire, wurtzite, electronic structure*

Recent developments in fabrication techniques and extensive investigations of physical properties of III−V semiconductor nanowires (NWs) have exposed their potential for a wide range of applications in electronics and photonics.[1−7] The use of NWs in such devices provide potential advantages over their planar counterparts due to, for example, improved band gap tuning, facilitated strain relaxation, increased tolerance of defects, lower material consumption, and, therefore, lower costs. Moreover, the one-dimensional (1D) nanostructure architecture allows one to extend band structure engineering beyond quantum confinement effects by utilizing formation of different crystal phases that can be synthesized in NWs but are thermodynamically unfavorable in bulk materials and related two-dimensional structures. Indeed, though the majority of bulk III−V materials such InP, GaP, and GaAs can only be grown with the zinc-blende (ZB) crystals structure, III−V NWs can also be synthesized either with the purely wurtzite (WZ) lattice structure or with controlled WZ and ZB segments, by carefully tuning growth parameters (such as V/III ratio, growth temperature, etc.).[8−10] Since the ZB and WZ phases typically exhibit different bandgap energies, such controlled polytypism provides an attractive opportunity for the realization of ZB-WZ heterostructures and polytypic superlattices within a NW made of a single semiconductor material.[9−14] This gives access not only to new interesting physical phenomena but also to fabrication of novel types of nanodevices. On the other hand, it was also demonstrated[12,15−17] that random polytypism and presence of randomly distributed rotational twin planes and stacking faults perpendicular to the growth direction may cause a detrimental impact on optical and electronic properties of NWs as they could lead to enhanced electron scattering, reduced quantum efficiency and carrier lifetime, etc. It is,

Received: March 17, 2015
Revised: May 13, 2015
Published: May 19, 2015

DOI: 10.1021/acs.nanolett.5b01054
Nano Lett. 2015, 15, 4052−4058

therefore, of crucial importance to understand the influence of local variations in the crystal structure of NWs on their fundamental physical properties.

Such information has recently been obtained in a number of III−V NWs based on direct bandgap semiconductors, such GaAs, GaN, and InP,[11,14,18,19] largely from extensive optical studies that utilized high radiative efficiency of these materials. On the other hand, similar studies devoted to WZ or polytypic gallium phosphide nanowires remains scarce,[20,21] in spite of the fact that GaP has the smallest lattice mismatch to Si (less than 0.4% at room temperature) and is, therefore, one of the best candidates for integration of photonics based on III−V materials with planar silicon technology. A major obstacle here is a low radiative efficiency of this indirect bandgap semiconductor and, therefore, a lack of radiative transitions related to free exciton or band-to-band recombination, which are often used to monitor electronic states caused by different lattice polytypes within NWs.[11,14,17,19] In principle, due to zone folding effects, the bandgap character of WZ GaP has been theoretically predicted[22−24] to change to a pseudodirect one with the lowest Γ_{8c} conduction band (CB) minimum (CBM) that is derived from the folded L_{6c} states of ZB. However, important issues on whether this should lead to an improved radiative efficiency of WZ GaP and also what is the bandgap energy of this material remain controversial.[20−24] For example, though the first principle calculations[22,24] have concluded that WZ GaP is a poor light emitter as the direct optical transitions between Γ_{8c} CBM and the valence band (VB) states are electric-dipole forbidden, the opposite conclusion was reached from transient photoluminescence (PL) measurements.[21] Also not known are effects of structural defects, such as stacking faults and twins, on the NWs optical quality.

In this paper we address these important issues by correlative studies of structural and optical properties of individual Ga(N)P-based NWs. The structural properties were monitored by aberration-corrected transmission electron microscopy (AC-TEM), whereas the optical properties were studied by cathodoluminescence (CL) spectroscopy. In order to improve the radiative efficiency of the wires, a small amount (up to 2%) of nitrogen was incorporated into GaP to form GaP/GaNP core/shell structures with the optically active shell layer of GaNP (see Methods for a detailed description of the samples structure). According to previous studies of bulk and two-dimensional GaNP, this material has a significantly higher oscillator strength of optical transitions caused by strong N-induced perturbations of the CB states which brings the Γ-character to the CB minimum of the formed alloy.[25] Our recent studies have demonstrated excellent optical quality of such GaP/GaNP NWs evident, e.g., from the observation of strong PL emissions over a wide temperature range with a significantly higher efficiency than that offered by GaP NWs.[26,27] We have also shown that the GaNP-based NWs structures are potentially important for novel optoelectronic applications, i.e., as a nanoscale light source that emits linearly polarized light with the polarization direction perpendicularly to the wire axis even in ZB nanowires[28] or for light harvesting utilizing energy upconversion.[29]

In order to determine the crystal structure of the investigated NWs that were grown by molecular beam epitaxy (MBE) on Si substrates, the NW structure was investigated by TEM. In general, both GaP and GaP/GaNP core/shell NWs are found to predominantly exhibit the ZB structure with a rather high density of randomly nucleated twin planes perpendicular to the growth axis. Typical low-resolution TEM images of two GaP/GaNP NW are shown in Figure 1a and b. It is found that these

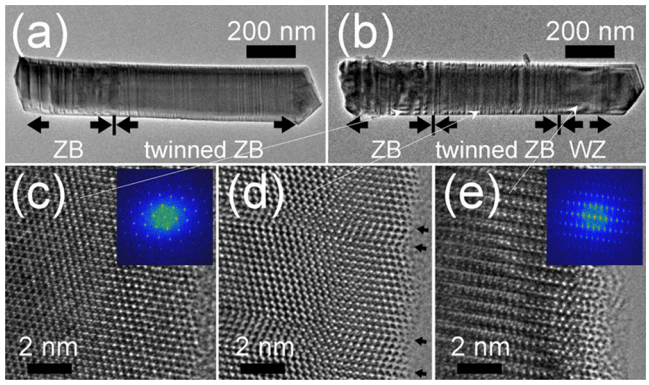

Figure 1. (a, b) Overview TEM images of GaP/GaNP core/shell NWs presenting different crystalline structures: (a) NW with predominantly ZB structure; (b) ZB NW with a large WZ inclusion. (c, d, e) Atomically resolved TEM images from different segments of the single GaP/GaNP NW shown in b: (c) the ZB segment; (d) the segment with twins in the ZB structure (the twinned planes have been marked with arrows); (e) the WZ segment. The dashed arrows indicate the exact spatial positions at which the atomically resolved images were taken. The insets in (c) and (e) show the fast Fourier transformation of the corresponding images.

NWs were grown from the ZB phase with few inclusions of twin planes initially. Atomically resolved TEM images of these regions demonstrate a high crystalline quality, as presented in Figure 1c with a corresponding fast Fourier transformation shown in the inset. Further NW growth resulted in a progressively increasing density of nucleated twin planes, as can be seen from the presence of mirrored domains—see Figure 1d, where positions of individual twin planes are indicated by the arrows. These twin planes can be formed in GaP due to the fact that the formation energy of a twinned layer is only slightly higher than that of the regular lattice.[30] Close to the top of the NWs, formation of a WZ segment is also found. In the case of the GaNP/GaP NW shown in Figure 1a, the WZ segment is about 3 nm long (not shown) and the total contribution of the WZ phase is about 0.3% of the total volume. This is characteristic for the majority of the studied GaP and GaP/GaNP NWs, where the WZ contribution is found to be below 2%. On the other hand, in some of the wires, such as that shown in Figure 1b, WZ segments can extend to up to 150 nm in length. Interestingly, the WZ sections in all studied NWs are found to incorporate significantly fewer faults as compared with the ZB regions. An atomically resolved HRTEM image of this WZ area is shown in Figure 1e, including a fast Fourier transformation of the image.

To understand effects of the revealed polytypism on optical properties and band structure of Ga(N)P, spatially resolved CL measurements were performed on the same NWs that were characterized by TEM. For these purposes, the NWs with a large WZ inclusion were chosen. The representative results from such measurements of the nanowires with the nitrogen content [N] = 0.9% are summarized in Figure 2, which shows the CL spectra c−d collected from different areas of the NW together with the corresponding scanning electron microscopy (a) and TEM (b) images. The CL spectra were obtained by scanning the electron beam along the NW axis. All spectra contain a broad CL band that has a rather asymmetric line

DOI: 10.1021/acs.nanolett.5b01054
Nano Lett. 2015, 15, 4052−4058

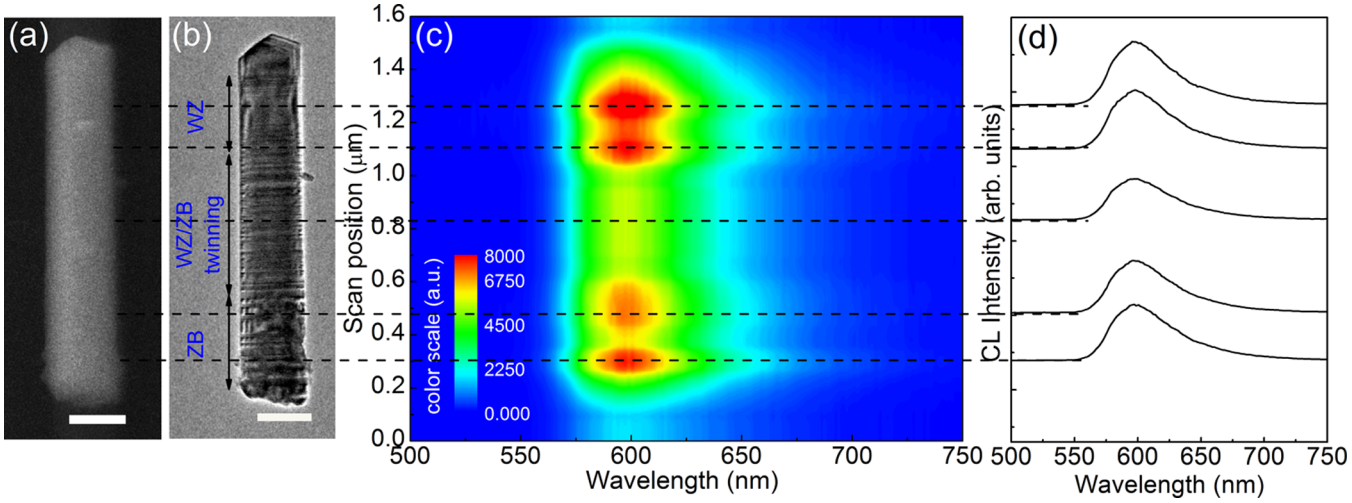

Figure 2. (a) SEM and (b) TEM images of a GaP/$GaN_{0.009}P_{0.991}$ NW with a large WZ inclusion. The scale bar is 200 nm. (c) CL line-scan image measured at 50 K along the axis of the same NW as shown in (a) and (b). The CL emission intensity is displayed as a function of the wavelength and emission position along the line-scan. The linear color scale is given in arbitrary units. (d) The corresponding CL spectra collected from the regions of the NW, as indicated by the horizontal dashed lines.

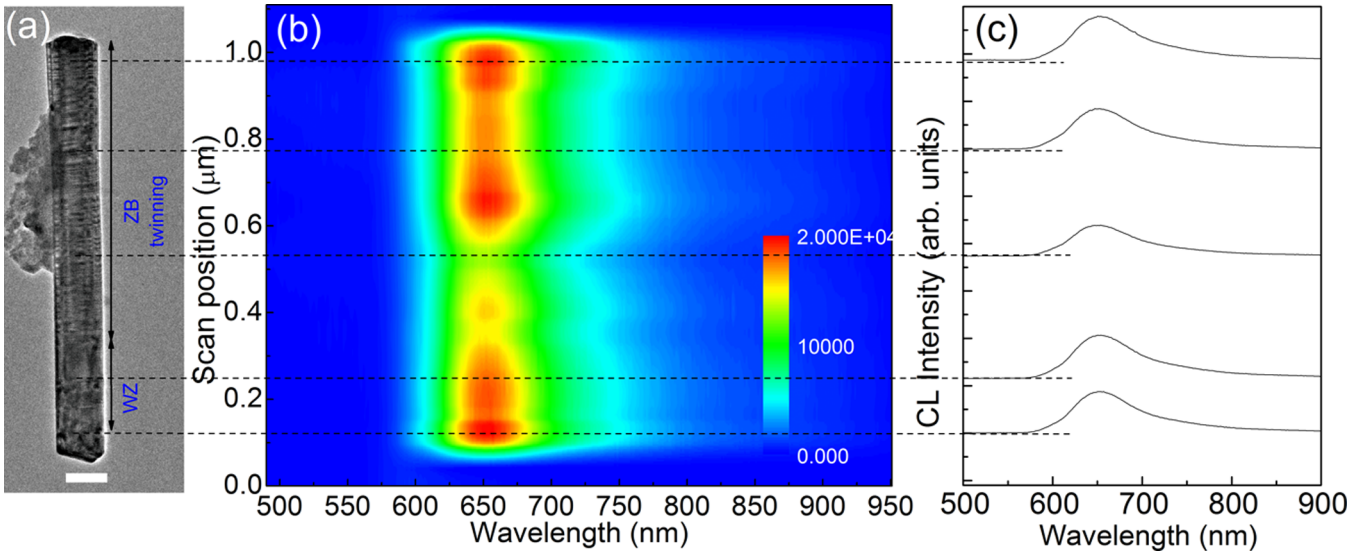

Figure 3. (a) TEM image of a GaP/$GaN_{0.019}P_{0.98}$ NW with a large WZ inclusion. The scale bar is 200 nm. (b) CL line-scan image measured at 50 K along the axis of the same NW as shown in (a). The CL emission intensity is displayed as a function of the wavelength and emission position along the line-scan. The linear color scale is given in arbitrary units. (c) The corresponding CL spectra collected from the regions of the NW as indicated by the horizontal dashed lines.

shape and peaks at around 595 nm. This emission originates from the GaNP shell, as it could only be detected upon N incorporation.[26] According to the previous PL studies of planar GaNP epilayers[31−33] and GaNP-based NW structures,[26] such an asymmetric line shape with a large tail on the low-energy side of the spectrum is typical for radiative recombination of excitons trapped at various N-related localized cluster states. The high energy cutoff of the detected emission is determined by the alloy bandgap energy and can, hence, be used to reliably monitor nitrogen composition in the alloy, even though the detected CL is not due to the band-to-band recombination. From Figure 2c and d, no obvious shift in the CL spectra is observed along the NW axis, which indicates high uniformity of the N composition in the GaNP shell, at least within the spatial resolution of around 150 nm estimated from the excitation volume during the CL measurements. It is also noticeable that the CL intensity varies by about 40% between different regions and is the lowest within the central part of the NW. By comparing the results of the CL mapping (Figure 2c) with the overview TEM image shown in Figure 2b, it becomes apparent that the bright CL emission originates from the NW regions with a low density of structural defects. On the other hand, the decrease of the CL intensity in the central part of the NW correlates with an increased twins density (see also Figure S1 of the Supporting Information for the CL mapping of the NW shown in Figure 1a, where the effect of twinning on the CL intensity is even more pronounced). This in turn implies that either these structural defects directly act as effective non-radiative recombination (NRR) centers competing with the monitored emission, or they promote formation of various NRR point defects nearby them that is consistent with the previously reported results for III−V and II−VI NWs.[34−37]

DOI: 10.1021/acs.nanolett.5b01054
Nano Lett. 2015, 15, 4052−4058

Most remarkably, the CL spectra recorded from the WZ segment localized within the top region are found to be identical in shape and very similar in intensity to that measured from the ZB region with a lower twin density, which is located close to the bottom end of the wire. This implies that the change in the lattice structure from ZB to WZ does not affect properties of light emission in the GaNP alloy. The same trend is observed for all investigated NWs independent of the N content, as can be seen, for example, from Figure 3 where results of CL mapping of a GaP/$GaN_{0.019}P_{0.981}$ NW with a large WZ inclusion are shown. The somewhat higher CL intensity (within 10−20%) in the WZ regions could be attributed to a lower density of structural defects in these areas.

In order to further elucidate effects of the revealed polymorphism on the optical properties, we performed temperature-dependent CL measurements. The corresponding results are summarized in Figure 4, taking as an example the ZB

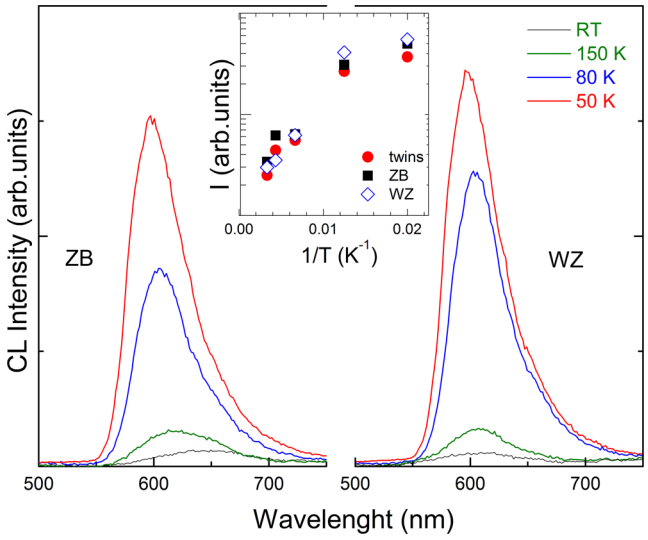

Figure 4. Temperature-dependent CL spectra measured from the ZB and WZ segments of the GaP/$GaN_{0.019}P_{0.98}$ NW shown in Figure 2. The inset show Arrhenius plots of the integrated CL intensity (I) measured from the spatial regions of the wire with distinctly different lattice structures as indicated in the figure.

and WZ segments of the GaP/$GaN_{0.009}P_{0.991}$ NW shown in Figure 2. Independent of the local lattice structure, increasing temperature is found to cause overall quenching of the CL intensity accompanied by a red shift of the CL emission band. The latter is commonly observed in planar GaNP alloys and reflects thermal depopulation of the N-related localized states, which starts from the states that are shallowest in energy (i.e., correspond to high-energy CL components).[31,32] Interestingly, differences in the CL intensity recorded from structurally different NW regions (i.e., twinned vs ZB or WZ segments) become less pronounced at elevated temperatures, as can clearly be seen from the Arrhenius plots of the spectrally integrated CL intensities shown in the inset of Figure 4. This finding suggests that the overall quenching of the emission intensity at elevated temperatures is caused by activation of NRR centers that are uniformly distributed over the wire and are, therefore, not related to the revealed structural defects. The probable candidates for these thermally activated NRR centers are point defects that play a detrimental role in light intensity of both GaNP nanowires and epilayers, as was unambiguously established from our optically detected magnetic resonance studies.[27,38,39]

To illustrate the effect of N on the optical properties of Ga(N)P NWs, results from low-temperature CL measurements of the studied GaP and GaP/GaNP core/shell nanowires with the N composition varied between 0.9 and 1.9% are shown in Figure 5. Due to an indirect bandgap, luminescence spectra

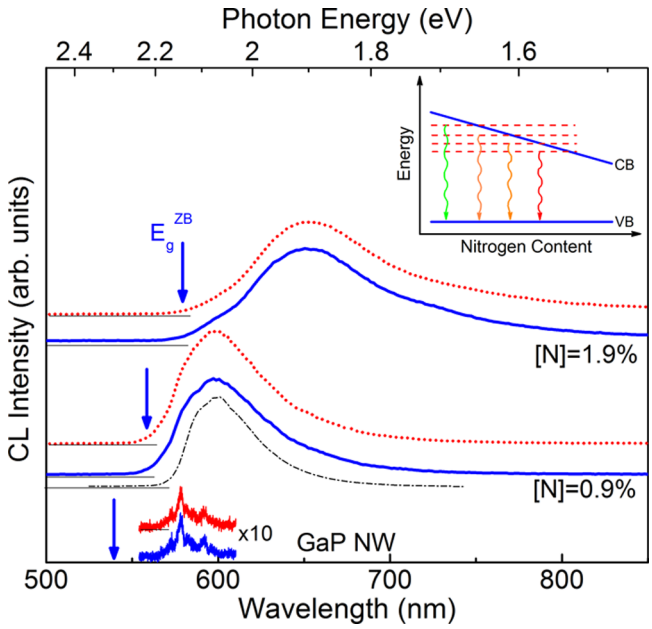

Figure 5. Normalized CL spectra collected from the ZB (solid blue lines) and the WZ (red dotted lines) sections of the GaP NW and the GaP/GaNP NWs with [N] = 0.9% and 1.9%. Also shown is a PL spectrum from a ZB $GaN_{0.009}P_{0.991}$ epilayer (the black dash-dotted line). The CL spectra of the N-containing NWs were measured at 50 K, whereas a lower measurement temperature of 30 K was used to record the emission from the GaP wires, due to strong thermal quenching of the monitored emission at higher temperatures. The spectra are vertically offset for clarity, as indicated by horizontal lines. The vertical arrows mark the energy position of the band gap of ZB GaP with the corresponding nitrogen content. An energy diagram is schematically shown in the inset.

from ZB GaP usually contain various BE lines that can only be detected at low temperatures. Such optical behavior is indeed observed in the studied GaP NWs where the CL emission is dominated by a series of rather week lines due to BE transitions that can only be detected at $T < 40$ K: see Figure 5. Though the exact origin of this emission is still unknown, it was never reported in bulk GaP but was observed in ZB GaP vapor-grown needles.[40] This may indicate that these BE transitions are related to the presence of defects characteristic for 1D structures. Upon alloying with nitrogen, the emission spectra become dominated by excitons bound to various N-related cluster states, which have a strong admixture of the Γ character and, hence, a high radiative efficiency.[41−43] Consistently, the CL intensity increases in the studied GaNP/GaP NWs as compared with that in the N-free GaP wires - see Figure 5. The observed increase cannot be chiefly related to the difference in the growth mode between the GaNP shell layer (step-mediated growth) and the GaP wires (vapor−liquid−solid (VLS) growth), since a similar increase of the radiative efficiency upon N incorporation was also observed in VLS-grown GaNP NWs (see Figure S2 of the Supporting Information). We also

DOI: 10.1021/acs.nanolett.5b01054
Nano Lett. 2015, 15, 4052−4058

note that the spectral shape of the CL emission from the GaNP NWs is identical to that in the ZB GaNP epilayers with the same [N] (shown by the black dashed-dotted curve in Figure 5), which implies that formation of structural defects does not affect the origin of the monitored optical transitions. From Figure 5, it is also noticeable that the CL emission exhibits a red shift upon N incorporation. The reason for this red shift is as follows. Due to the huge bowing of the GaNP bandgap energy with increasing [N], dominated by the downshift of the CB edge, defect levels from different N centers and clusters one-by-one become resonant with the CB states[31,32,41] as schematically shown in the inset of Figure 5. This results in disappearance of the related optical transitions and, consequently, a gradual red shift of the monitored emission as observed experimentally. As expected, the high-energy cutoff of the monitored emission is determined by the energy position of the CB edge (or the bandgap energy). The latter is indicated by the arrows in Figure 5, estimated based on the band-anticrossing (BAC) model[43,44] using the known parameters for ZB GaNP. The emission line width, on the other hand, is determined by energy distribution of the N-related localized states determined by local fluctuations in the N content. From Figure 5, these fluctuations become more significant in the nanowires with a higher N composition (e.g., [N] = 1.9% shown in Figure 5) leading to the observed broadening of the CL spectra. All of the aforementioned changes are identical to those documented previously in planar structures.[25,41−43]

In contrast to ZB Ga(N)P, the band structure of WZ Ga(N)P is significantly less studied. In fact it remains as a subject of ongoing discussions[20−24] even in the case of pure WZ GaP and is completely unknown for GaNP alloys. Our results from the performed CL mapping of the Ga(N)P NWs (Figures 2 and 3) clearly show that both WZ and ZB phases have very similar optical properties, judging from the spectral line shape, energy positions and also intensities of the detected CL emission. First of all, these findings imply that both polytypes have a very similar bandgap energy E_g, as an increase (decrease) of the bandgap should otherwise lead to a corresponding blue (red) shift of the GaNP emission. This remains true even for the N-free GaP wires. Second, in spite of the better structural quality of the WZ segments, similar emission intensities are observed from the WZ and ZB Ga(N)P segments. This suggest that WZ GaP does not acquire a true direct-bandgap character. This is because the radiative efficiency of optical transitions in direct bandgap semiconductors should be substantially higher than that in indirect bandgap materials, typically by about 2−3 orders of magnitude.[45] Because of the band enhancement effect,[46] this should remain valid even for BE optical transitions such as isoelectronic excitons bound to different N clusters monitored in the studied GaNP NWs or BE transitions in GaP. Such enhancement, however, is not observed experimentally—see Figure 5. We note that Assali et al.[21] have previously reported a strong enhancement (by at least 65 times) and a red shift of the PL emission by 0.23 eV in WZ GaP NWs as compared with that in bulk ZB GaP. As can be seen from Figure 5, none of these effects could be detected in our structures, where identical CL spectra are detected from the WZ and ZB segments. Though the exact reason for this contradiction is unknown at present, it should be pointed out that the optical measurements performed in ref 21 were restricted to WZ nanowires without studying reference NWs with the ZB structure synthesized under similar conditions in the same growth chamber (a bulk ZB GaP substrate was used instead). Moreover, structural and optical measurements in this earlier work were performed on different wires, whereas in our case they were correlated within the same NW.

For the GaP NWs, the aforementioned experimental findings are generally consistent with the results of local density band-structure calculations.[22,24] It was theoretically predicted that in case when the lowest X_{6c} minimum in a ZB compound lies close in energy with the L_{6c} states, the bandgap of such material will become pseudodirect in the WZ structure with the lowest Γ_{8c} CB state at the zone center that is derived from the zone folded L_{6c} states. Consequently, the material will remain optically inactive in the WZ structure, as the direct optical transitions that define the absorption edge are dipole-forbidden.[22,24] This scenario was proposed for GaP where the L_{6c} state is located at 2.44 eV relative to the VB maximum, which is close to the energy position of the X_{6c} CBM at 2.35 eV. The calculated Γ_{8c} energy in WZ was found to be only slightly below that of the X_{6c} CBM in ZB, i.e., by about 0.06−0.2 eV.[23,24] Though our results from the WZ GaP does not allow us to accurately determine its bandgap energy E_g^{WZ}, they place the lowest bound of E_g^{WZ} at 2.19 eV at 30 K, which corresponds to the highest energy of the detected BE emission (without taking into account the exciton binding energy). We also note that our present studies cannot rule out the possibility that the lowest CB minimum in WZ GaP remains at the X point of the Brillouin zone.

As to the GaNP alloys, the results of CL mapping prove that the WZ and ZB polytypes have the same bandgap energy as the high energy cutoff of the CL spectra is identical in both cases. This finding can be understood as follows. Phenomenologically, the change of the bandgap energy of GaP upon N incorporation can be described within the band anticrossing model, which suggests that the energy position of the CB edge can be adequately modeled by considering an anticrossing interaction between the extended Γ CB state of the GaP matrix and the localized state (E_N) of a substitutional N_P center.[43,44] The strength of this interaction is mainly determined by the energy distance between the Γ CB minimum and the E_N position. In ZB, the interacting host states are the Γ_{6c} CB states, whereas their equivalent in WZ are the Γ_{7c} CB states that are theoretically predicted[22,24] to be located almost at the same energy as the Γ_{6c} states in ZB. To explain the observed independence of the GaNP bandgap energy on the crystal structure we then need to assume the same energy position of the N-related states in the WZ and ZB materials. This assumption is probably quite reasonable taking into account the deep-level character of these states and the identical spectral positions of the corresponding BE emissions observed experimentally.

In conclusion, we have employed low-temperature CL mapping correlated with AC-TEM measurements performed on the same nanowires and temperature-dependent CL measurements to investigate effects of structural polytypism on optical properties of MBE-grown GaP and GaP/GaNP core/shell NW structures. It is found that structural defects, such as rotational twins in ZB GaNP, have detrimental effects on light emission intensity at low temperatures. This implies that either these defects are directly involved in nonradiative recombination processes or they facilitate formation of point defects that act as efficient NRR centers. On the other hand, the contribution of the structural defects becomes less significant at elevated temperatures when the NRR processes involving point defects dominate. The formation of the WZ

DOI: 10.1021/acs.nanolett.5b01054
Nano Lett. 2015, 15, 4052−4058

phase does not change the intensity of the monitored CL either in GaP or in the GaNP alloy. Considering a better structural quality of the WZ segments, this finding is consistent with the results of the first principle calculations[22,24] suggesting that the fundamental band-to-band transitions in WZ GaP remain dipole forbidden in spite of zone folding. Moreover, the bandgap energy of WZ GaP is concluded to be above 2.19 eV at 30 K (without taking into account the exciton binding energy). We also show that the change in the lattice structures does not affect the bandgap energies of the GaNP alloys, at least within the range of nitrogen composition [N] < 2.0% studied in this work. Both WZ and ZB GaNP are found to have a significantly higher efficiency of radiative recombination as compared with that in the parental GaP, promising for potential applications of GaNP NWs as efficient nanoscale light emitters within the amber-red spectral range.

Methods. The investigated GaP NWs and GaP/GaNP core/shell NWs were grown by gas-source molecular beam epitaxy (GS MBE) on Si(111) substrates as reported previously.[47] The GaP NWs were synthesized in a Ga-catalyzed vapor−liquid−solid (VLS) growth mode at a substrate temperature T_{sub} of 580 °C with a V/III flux ratio of 1.5. The same growth conditions were used for the growth of core regions in the coaxial NW heterostructures. The GaNP shell was fabricated via the step-mediated growth at a lower substrate temperature T_{sub} of 520 °C and a V/III flux ratio of 2.5. The nitrogen composition in the shell was varied between 0.6 and 2.0% by changing the power of the rf-plasma and the nitrogen flux. The nitrogen content in the resulting core/shell NWs was estimated by comparing the PL data with the band anticrossing model.[43] The performed SEM measurements have shown that the NWs are oriented perpendicular to the substrate plane and exhibit a hexagonal cross-section, indicating that they were epitaxially grown following the [111] crystallographic orientation of Si substrates. The lateral facets of these NW are found to belong to the{1$\bar{1}$0} crystallographic family. The NWs are uniform in sizes and have an axial length of about 2−2.5 μm, an average diameter of 110 nm for the GaP NWs and approximately 220 nm for the GaP/GaNP core/shell structure.

Samples for TEM and CL characterization were prepared by direct transfer of the NWs onto a carbon/copper grid. The crystal structure of the NWs was analyzed by AC-TEM using the Linköping double corrected Titan^3 60−300 microscope. For these purposes the nanowires were mechanically transferred onto TEM grids. The structure of the NWs was manually characterized from top to bottom at high magnification and high resolution. Structure images of ZB and WZ regions were identified and recorded at high magnification, while overview images were obtained by zooming out from the identified regions. Spatially resolved measurements of the CL spectra along the NW axis were performed in a dedicated setup using a Leo 1550 Gemini SEM microscope equipped with a He-cooling stage. The CL system was operated with either a photomultiplier tube for monochromatic imaging or a charge-coupled device (CCD) detector to record CL spectra. Both CL and SEM images were recorded simultaneously. CL mapping was performed by scanning an electron beam along the NW with the acceleration voltage of 5 kV. Based on performed Monte Carlo simulations, the maximum concentration of the electron−hole pairs (and, therefore, the CL intensity) under these conditions was generated from a depth of 50 nm, whereas about 80% of the CL intensity emerged from the depth of 0−140 nm. Taking into account strong localization effects in the studied nanowires due to fluctuations in N composition and structural defects, this determines the spatial resolution during the CL measurements as being around 140 nm. For each N composition, the CL mapping was done on 3−8 nanowires that were first characterized by TEM.

■ ASSOCIATED CONTENT

Supporting Information

Description of additional experimental results. The Supporting Information is available free of charge on the ACS Publications website at DOI: 10.1021/acs.nanolett.5b01054.

■ AUTHOR INFORMATION

Corresponding Author

*E-mail: iribu@ifm.liu.se.

Author Contributions

The samples were grown by S.S. and Y.K. under supervision of C.W.T. TEM images were acquired by P.O.Å. A.D. carried out the CL measurements and analyzed the data with guidance from W.M.C. and I.A.B. I.A.B. wrote the final version of the manuscript, with contributions from the coauthors.

Notes

The authors declare no competing financial interest.

■ ACKNOWLEDGMENTS

Financial support by the Swedish Energy Agency (grant no. P40119-1) is greatly appreciated. The nanowire growth is supported by the U.S. National Science Foundation under Grant no. DMR-0907652 and DMR-1106369. S.S. is partially funded by a Royal Government of Thailand Scholarship. The Knut and Alice Wallenberg Foundation is gratefully acknowledged for funding of the Electron Microscopy laboratory in Linköping.

■ REFERENCES

(1) Wang, J.; Gudiksen, M. S.; Duan, X.; Cui, Y.; Lieber, C. M. *Science* **2001**, *293*, 1455−1457.

(2) Gudiksen, M. S.; Lauhon, L. J.; Wang, J.; Smith, D. C.; Lieber, C. M. *Nature* **2002**, *415*, 617−620.

(3) Yan, R. X.; Gargas, D.; Yang, P. D. *Nat. Photonics* **2009**, *3*, 569−576.

(4) Wallentin, J.; Anttu, N.; Asoli, D.; Huffman, M.; Aberg, I.; Magnusson, M. H.; Siefer, G.; Fuss-Kailuweit, P.; Dimroth, F.; Witzigmann, B.; Xu, H. Q.; Samuelson, L.; Deppert, K.; Borgström, M. T. *Science* **2013**, *339*, 1057−1060.

(5) Saxena, D.; Mokkapati, S.; Parkinson, P.; Jiang, N.; Gao, Q.; Tan, H. H.; Jagadish, C. *Nat. Photonics* **2013**, *7*, 963−968.

(6) Tomioka, K.; Yoshimura, M.; Fukui, T. A. *Nature* **2012**, *488*, 189−192.

(7) Thelander, C.; Agarwal, P.; Brongersma, S.; Eymery, J.; Feiner, L. F.; Forchel, A.; Scheffler, M.; Riess, W.; Ohlsson, B. J.; Gösele, U.; Samuelson, L. *Mater. Today* **2006**, *9*, 28−35.

(8) Caroff, P.; Dick, K. A.; Johansson, J.; Messing, M. E.; Deppert, K.; Samuelson, L. *Nat. Nanotechnol.* **2009**, *4*, 50−55.

(9) Algra, R. E.; Verheijen, M. A.; Borgström, M. T.; Feiner, L.-F.; Immink, G.; van Enckevort, W. J. P.; Vlieg, E.; Bakkers, E. P. A. M. *Nature* **2008**, *456*, 369−372.

(10) Joyce, H. J.; Wong-Leung, J.; Gao, Q.; Hoe Tan, H.; Jagadish, C. *Nano Lett.* **2010**, *10*, 908−915.

(11) Spirkoska, D.; Arbiol, J.; Gustafsson, A.; Conesa-Boj, S.; Glas, F.; Zardo, I.; Heigoldt, M.; Gass, M. H.; Bleloch, A. L.; Estrade, S.; Kaniber, M.; Rossler, J.; Peiro, F.; Morante, J. R.; Abstreiter, G.; Samuelson, L.; Fontcuberta i Morral, A. *Phys. Rev. B* **2009**, *80*, 245325.

(12) Bao, J.; Bell, D. C.; Capasso, F.; Wagner, J. B.; Mårtensson, T.; Trägårdh, J.; Samuelson, L. *Nano Lett.* **2008**, *8*, 836−841.

DOI: 10.1021/acs.nanolett.5b01054
Nano Lett. 2015, 15, 4052−4058

(13) Bolinsson, J.; Caroff, P.; Mandl, B.; Dick, K. A. *Nanotechnology* **2011**, *22*, 265606.
(14) Akopian, N.; Patriarche, G.; Liu, L.; Harmand, J.-C.; Zwiller, V. *Nano Lett.* **2010**, *10*, 1198−1201.
(15) Woo, R. L.; Xiao, R.; Kobayashi, Y.; Gao, L.; Goel, N.; Hudait, M. K.; Mallouk, T. E.; Hicks, R. F. *Nano Lett.* **2008**, *8*, 4664−4669.
(16) Perera, S.; Fickenscher, M. A.; Jackson, H. E.; Smith, L. M.; Yarrison-Rice, J. M.; Joyce, H. J.; Gao, Q.; Tan, H. H.; Jagadish, C.; Zhang, X.; Zou, J. *Appl. Phys. Lett.* **2008**, *93*, 053110.
(17) Parkinson, P.; Joyce, H. J.; Gao, Q.; Tan, H. H.; Zhang, X.; Zou, J.; Jagadish, C.; Herz, L. M.; Johnston, M. B. *Nano Lett.* **2009**, *9*, 3349−3353.
(18) Jahn, U.; Lähnemann, J.; Pfüller, C.; Brandt, O.; Breuer, S.; Jenichen, B.; Ramsteiner, M.; Geelhaar, L.; Riechert, H. *Phys. Rev. B* **2012**, *85*, 045323.
(19) Jacopin, G.; Rigutti, L.; Largeau, L.; Fortuna, F.; Furtmayr, F.; Julien, F. H.; Eickhoff, M.; Tchernycheva, M. *J. Appl. Phys.* **2011**, *110*, 064313.
(20) Zhang, Z.; Senz, S.; Zhao, F.; Chen, L.; Gao, X.; Liu, J.-M. *RSC Adv.* **2012**, *2*, 8631−8636.
(21) Assali, S.; Zardo, I.; Plissard, S.; Kriegner, D.; Verheijen, M. A.; Bauer, G.; Meijerink, A.; Belabbes, A.; Bechstedt, F.; Haverkort, J. E. M.; Bakkers, E. P. A. M. *Nano Lett.* **2013**, *13* (4), 1559−1563.
(22) Yeh, C.-Y.; Wei, S.-H.; Zunger, A. *Phys. Rev. B* **1994**, *50* (4), 2715−2718.
(23) De, A.; Pryor, C. E. *Phys. Rev. B* **2010**, *81*, 155210.
(24) Belabbes, A.; Panse, C.; Furthmüller, J.; Bechstedt, F. *Phys. Rev. B* **2012**, *86*, 075208.
(25) *Physics and applications of dilute nitrides*; Buyanova, I. A., Chen, W. M., Eds.; Taylor & Francis: New York, 2004.
(26) Dobrovolsky, A.; Stehr, J. E.; Chen, S. L.; Kuang, Y. J.; Sukrittanon, S.; Tu, C. W.; Chen, W. M.; Buyanova, I. A. *Appl. Phys. Lett.* **2012**, *101*, 163106.
(27) Stehr, J. E.; Dobrovolsky, A.; Sukrittanon, S.; Kuang, Y. J.; Tu, C. W.; Chen, W. M.; Buyanova, I. A. *Nano Lett.* **2015**, *15* (1), 242−247.
(28) Filippov, S.; Sukrittanon, S.; Kuang, Y.; Tu, C. W.; Persson, P. O. Å.; Chen, W. M.; Buyanova, I. A. *Nano Lett.* **2014**, *14*, 5264−5269.
(29) Dobrovolsky, A.; Sukrittanon, S.; Kuang, Y. J.; Tu, C. W.; Chen, W. M.; Buyanova, I. A. *Small* **2014**, *10*, 4403−4408.
(30) Gottschalk, H.; Patzer, G.; Alexander, H. *Phys. Status Solidi* **1978**, *45*, 207.
(31) Buyanova, I. A.; Rudko, G. Y.; Chen, W. M.; Xin, H. P.; Tu, C. W. *Appl. Phys. Lett.* **2002**, *80*, 1740−1742.
(32) Buyanova, I. A.; Chen, W. M.; Tu, C. W. *Solid-State Electron.* **2003**, *47*, 467−475.
(33) Liu, X.; Bishop, S. G.; Baillargeon, J. N.; Cheng, K. Y. *Appl. Phys. Lett.* **1993**, *63*, 208−210.
(34) Joyce, H. J.; Gao, Q.; Tan, H. H.; Jagadish, C.; Kim, Y.; Zou, J.; Smith, L. M.; Jackson, H. E.; Yarrison-Rice, J. M.; Parkinson, P.; Johnston, M. B. *Prog. Quantum Electron.* **2011**, *35*, 23−75.
(35) Titova, L. V.; Hoang, T. B.; Jackson, H. E.; Smith, L. M.; Yarrison- Rice, J. M.; Kim, Y.; Joyce, H. J.; Tan, H. H.; Jagadish, C. *Appl. Phys. Lett.* **2006**, *89*, 173126.
(36) Liu, Z.; Zhang, X.; Hark, S. K. *Cryst. Growth Des.* **2009**, *9*, 803−806.
(37) Svensson, C. P. T.; Mårtensson, T.; Trädgårdh, J.; Larsson, C.; Rask, M.; Hessman, D.; Samuelson, L.; Ohlsson, J. *Nanotechnol* **2008**, *19*, 305201.
(38) Thinh, N.; Vorona, I.; Buyanova, I.; Chen, W.; Limpijumnong, S.; Zhang, S.; Hong, Y.; Xin, H.; Tu, C.; Utsumi, A.; Furukawa, Y.; Moon, S.; Wakahara, A.; Yonezu, H. *Phys. Rev. B* **2005**, *71*, 125209.
(39) Dagnelund, D.; Vorona, I. P.; Vlasenko, L. S.; Wang, X. J.; Utsumi, A.; Furukawa, Y.; Wakahara, A.; Yonezu, H.; Buyanova, I. A.; Chen, W. M. *Phys. Rev. B* **2010**, *81*, 115334.
(40) Dean, P. J.; Thomas, D. G.; Frosch, C. J. *J. Phys. C: Solid State Phys.* **1984**, *17*, 747−762.
(41) Kent, P. R. C.; Zunger, A. *Phys. Rev. Lett.* **2001**, *86*, 2613−2616.
(42) Buyanova, I. A.; Pozina, G.; Bergman, J. P.; Chen, W. M.; Xin, H. P.; Tu, C. W. *Appl. Phys. Lett.* **2002**, *81*, 52−54.
(43) Shan, W.; Walukiewicz, W.; Yu, K. M.; Wu, J.; Ager, J. W.; Haller, E. E.; Xin, H. P.; Tu, C. W. *Appl. Phys. Lett.* **2000**, *76*, 3251−3253.
(44) Buyanova, I. A.; Izadifard, M.; Kasic, A.; Arwin, H.; Chen, W. M.; Xin, H. P.; Hong, Y. G.; Tu, C. W. *Phys. Rev. B* **2004**, *70*, 085209.
(45) Groves, W. O.; Herzog, A. H.; Cradord, M. G. *Appl. Phys. Lett.* **1971**, *19*, 184−186.
(46) Kash, J. A.; Collet, J. H.; Wolford, D. J.; Thompson, J. *Phys. Rev. B* **1983**, *27*, 2294−2300.
(47) Kuang, Y. J.; Sukrittanon, S.; Li, H.; Tu, C. W. *Appl. Phys. Lett.* **2012**, *100*, 053108.

DOI: 10.1021/acs.nanolett.5b01054
Nano Lett. 2015, 15, 4052−4058